



OPEN ACCESS

EDITED BY

Shuliang Zhang,
Nanjing Normal University, China

REVIEWED BY

Chi Yang,
Distinguished Professor of Nanjing
University of Information Science and
Technology, China
Albert Ossó,
University of Graz, Austria

*CORRESPONDENCE

Fasil M. Rettie,
✉ fasil.mequanint@uni-hohenheim.de

SPECIALTY SECTION

This article was submitted to
Atmosphere and Climate,
a section of the journal
Frontiers in Environmental Science

RECEIVED 19 December 2022

ACCEPTED 28 March 2023

PUBLISHED 09 May 2023

CITATION

Rettie FM, Gayler S, Weber TKD, Tesfaye K
and Streck T (2023), Comprehensive
assessment of climate extremes in high-
resolution CMIP6 projections
for Ethiopia.
Front. Environ. Sci. 11:1127265.
doi: 10.3389/fenvs.2023.1127265

COPYRIGHT

© 2023 Rettie, Gayler, Weber, Tesfaye
and Streck. This is an open-access article
distributed under the terms of the
[Creative Commons Attribution License
\(CC BY\)](https://creativecommons.org/licenses/by/4.0/). The use, distribution or
reproduction in other forums is
permitted, provided the original author(s)
and the copyright owner(s) are credited
and that the original publication in this
journal is cited, in accordance with
accepted academic practice. No use,
distribution or reproduction is permitted
which does not comply with these terms.

Comprehensive assessment of climate extremes in high-resolution CMIP6 projections for Ethiopia

Fasil M. Rettie^{1,2*}, Sebastian Gayler¹, Tobias K. D. Weber^{1,3},
Kindie Tesfaye⁴ and Thilo Streck¹

¹Institute of Soil Science and Land Evaluation, Biogeophysics, University of Hohenheim, Stuttgart, Germany, ²Ethiopian Institute of Agricultural Research (EIAR), Melkasa, Ethiopia, ³Soil Science Section, Faculty of Organic Agricultural Sciences, University of Kassel, Witzenhausen, Germany, ⁴International Maize and Wheat Improvement Center (CIMMYT), Addis Ababa, Ethiopia

Climate extremes have more far-reaching and devastating effects than the mean climate shift, particularly on the most vulnerable societies. Ethiopia, with its low economic adaptive capacity, has been experiencing recurrent climate extremes for an extended period, leading to devastating impacts and acute food shortages affecting millions of people. In face of ongoing climate change, the frequency and intensity of climate extreme events are expected to increase further in the foreseeable future. This study provides an overview of projected changes in climate extremes indices based on downscaled high-resolution (i.e., 10 × 10 km²) daily climate data derived from global climate models (GCMs). The magnitude and spatial patterns of trends in the projected climate extreme indices were explored under a range of emission scenarios called Shared Socioeconomic Pathways (SSPs). The performance of the GCMs to reproduce the observed climate extreme trends in the base period (1983–2012) was evaluated, the changes in the climate projections (2020–2100) were assessed and the associated uncertainties were quantified. Overall, results show largely significant and spatially consistent trends in the projected temperature-derived extreme indices with acceptable model performance in the base period. The projected changes are dominated by the uncertainties in the GCMs at the beginning of the projection period while by the end of the century proportional uncertainties arise both from the GCMs and SSPs. The results for precipitation-related extreme indices are heterogeneous in terms of spatial distribution, magnitude, and statistical significance coverage. Unlike the temperature-related indices, the uncertainty from internal climate variability constitutes a considerable proportion of the total uncertainty in the projected trends. Our work provides a comprehensive insight into the projected changes in climate extremes at relatively high spatial resolution and the related sources of projection uncertainties.

KEYWORDS

climate extremes, CMIP 6, Ethiopia, precipitation, SSPs, temperature, uncertainty, trend

1 Introduction

There is unequivocal and overwhelming evidence for the ongoing climate change. The projected 1.5°C increase in global average temperature by 2050s poses risks to humans and ecosystems (IPCC, 2022). The changing climate has manifested itself in higher climate extremes events (Myhre et al., 2019; Madakumbura et al., 2021). Climate extremes usually have more devastating effects than the mean shift in the climate. Expected increases in flash flood events following more frequent and extreme precipitation events, or droughts as a result of prolonged periods of extremely low precipitation are situations that may cost countries a huge price (IPCC, 2022). Extreme heat or cold waves have far-reaching socioeconomic and mental effects on the most vulnerable societies (IPCC, 2022). Since 2005, the world has witnessed 9 warmest years, and 2019 has been recorded as one of the three warmest years since the records have begun. This global phenomenon has significant implications, particularly for the most vulnerable part of the world's economy. Kemp et al. (2022) suspect that, together with other global threats, the changing climate may become catastrophic even at modest levels of warming.

Ethiopia's economy depends largely on agriculture and it is considered to be among the countries that are most vulnerable to climate extremes. The agricultural sector second contributes ~38% to the GDP (Gross Domestic Product) of the country but employs 67% of the population and contributes about 86% of export earnings (Eshetu and Mehare, 2020; World Bank, 2022b; World Bank, 2022c). Moreover, the largely subsistence agriculture relies on seasonal rains. The proportion of irrigated land was only 2.1% in 2018 (World Bank, 2022a) and agricultural mechanization was below 1% (Berhane et al., 2017). Ethiopia has faced recurrent climate extreme effects for a long period usually resulting in a devastating impact and leaving millions in acute food shortage (Kiros, 1991; Mohammed et al., 2018). The 2022 drought was one of the worst in 50 years, leaving 2.2 million livestock dead (FEWS NET, 2022). Considering the projected population of >200 million by 2050 (World Bank, 2022d), the challenge of comparable drought periods for the already vulnerable economy would be enormous. Against this background, detailed quantification of climate extremes is particularly relevant for Ethiopia.

For the past climate, studies have documented consistent increasing temperature trends both in mean and extremes in East Africa in general (Gebrechorkos et al., 2019b; Muthoni et al., 2019; Afuecheta and Omar, 2021) and Ethiopia in particular (Gummedi et al., 2018; Gebrechorkos et al., 2019b; 2019a). However, precipitation has been reported as inconsistent across the region (Viste et al., 2013; Tierney et al., 2015; Cattani et al., 2018; Gummedi et al., 2018). For instance, Tierney et al. (2015) documented unusual drying of March–May rainfall in East Africa during the past century. Meanwhile, their assessment based on 23 CMIP5 models by the end of the 21st century show largely increasing seasonal as well as annual precipitation totals under high emission (RCP 8.5) scenario (Tierney et al., 2015). Drying spring and summer seasons have also been reported for southern Ethiopia. The drying springs have affected most parts of the country (Viste

et al., 2013). However, local scale studies identified higher spatial variability both in the observed and projected climate trends, particularly for precipitation (Brown et al., 2017; Muthoni et al., 2019; Alaminie et al., 2021; Bayable et al., 2021). High spatial variability was also visible in past climate extremes (Cattani et al., 2018; Esayas et al., 2018; Ademe et al., 2020; Gemedo et al., 2021; Ali Mohammed et al., 2022; Birhan et al., 2022; Dendir and Birhanu, 2022). Understanding the time evolution of extreme climate events is of large interest for designing potential adaptation options and informed decision-making (Kemp et al., 2022). Ethiopia is characterized by diverse climate regimes modulated by its complex topography exerting strong elevation gradients (Diro et al., 2011; Van den Hendt et al., 2021), which require finer spatial resolution to produce relevant results (El Kenawy et al., 2016).

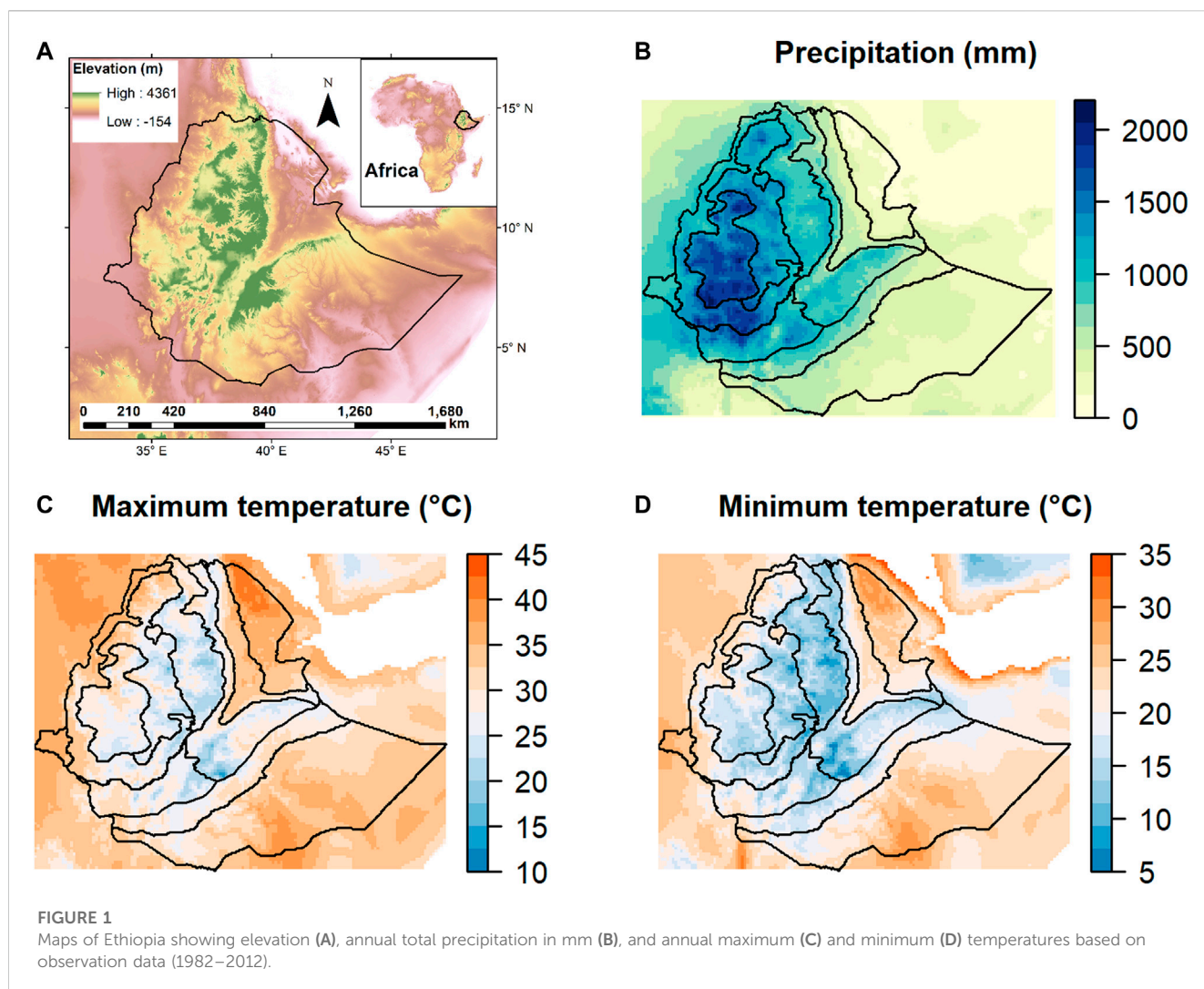
The basic sources of projected climate data are the Global Climate Models (GCMs) running on coarse spatial resolution at $> 70 \times 70 \text{ km}^2$. The projected data are highly uncertain, mainly due to the structural and parametrization differences among the models (Murphy et al., 2004; Her et al., 2019; Lee et al., 2021). Therefore, adaptation to climate extremes should be based on multi-model-based simulation at high spatial resolution taking into account several emission scenarios (Fatichi et al., 2016). For Ethiopia, these GCM projections were recently downscaled to $10 \times 10 \text{ km}^2$ spatial resolution for temperature and precipitation (Rettie et al., 2023). The data were derived from the most current GCMs in the Coupled Model Intercomparison Project Phase 6 (CMIP6) under three Shared Socioeconomic Pathways (SSPs) by employing a statistical downscaling technique (Hamlet et al., 2010; Maurer et al., 2010).

The present study provides an overview of observed and projected changes in climate extremes indices derived from the downscaled high-resolution daily climate data by Rettie et al. (2023). For this, we compared the historical simulation of the CMIP6 models and analyzed the temporal and spatial distributions of projected changes. The skill of the individual models in reproducing the observed trends of climate extremes in the base period (i.e., 1983–2012) was evaluated, and the uncertainties associated with the projected (i.e., 2020–2100) trends were quantified.

2 Materials and methods

2.1 Climate data

The climate hazards group database provides free daily climate data with a $5 \times 5 \text{ km}^2$ spatial resolution with quasi-global coverage (50°S–50°N, <ftp://ftp.chg.ucsb.edu/pub/org/chg/products/>). Daily climate data is available for the study area (Figure 1A) from CHIRPS (Climate Hazards Group InfraRed Precipitation with Stations) for precipitation (Funk et al., 2015) and from CHIRTS (Climate Hazards Group InfraRed Temperature with Stations) for temperature (Verdin et al., 2020) (Figures 1B–D). The data were generated in several stages by blending satellite records and *in situ* station data and are available since 1981 for precipitation and from



1983 to 2016 for temperature. The data has been evaluated for its ability to reliably reproduce the climatology and major meteorological systems of Ethiopia (Dinku et al., 2018; Belete et al., 2020; Taye et al., 2020; Kabite Wedajo et al., 2021; Malede et al., 2022) and other regions (Zambrano-Bigiarini et al., 2017; Saeidizand et al., 2018; Muthoni et al., 2019; Muthoni, 2020).

This work was conducted based on previously downscaled climate projections covering the period of 2020–2100 from a list of CMIP6 GCMs under three emission scenarios known as shared socioeconomic pathways (SSPs) (Rettie et al., 2023). The data was produced by applying a geospatial statistical downscaling technique to downscale the original coarse spatial resolution (i.e., > 70 × 70 km²) GCM outputs to 10 × 10 km² spatial resolution covering entire Ethiopia (3°N–15°N and 32°E–48°E). The data includes projections of temperature and precipitation from 13 to 9 CMIP6 GCMs, respectively (Table 1). For a detailed description of the downscaling procedure and evaluation see there. In this study, we considered the downscaled climate projections datasets under three SSPs. The selected SSPs are SSP2-4.5, SSP3-7.0, and SSP5-8.5, which represent medium,

medium-high, and high-forcing scenarios based on middle-of-the-road, regional rivalry, and fossil-fueled socioeconomic development scenarios, respectively (O'Neill et al., 2017; Meinshausen et al., 2020). The emission scenarios span a broad range of CO² concentration, with radiative forcing level of 4.5 Wm⁻² and 8.5 Wm⁻² by 2100 for SSP2-4.5 and SSP5-8.5, respectively (IPCC, 2021).

2.2 Climate extreme indices

Table 2 lists the 23 climate extreme indices investigated in this study. The indices were among the 27 climate change indicators which were developed by the Expert Team on Climate Change Detection, Monitoring Indices (ETCCDMI) and have been recommended by the World Meteorological Organization (WMO) (Zhang et al., 2011). The R package *climdex.pcic* (Pacific Climate Impacts Consortium (2020), <http://cran.r-project.org/web/packages/climdex.pcic/index.html>) was used to derive the climate indices at 10 × 10 km² grid

TABLE 1 List of GCMs and availability of data with respect to maximum (Tmax) and minimum (Tmin) temperatures and precipitation (Pr).

Model name	Institution name	Tmax	Tmin	Pr	Resolution (lon. by lat.)
ACCESS-CM2	Commonwealth Scientific and Industrial Research Organization (CSIRO) and Bureau of Meteorology (BOM), Australia	✓	✓	✓	1.9° × 1.3°
ACCESS-ESM1-5	Commonwealth Scientific and Industrial Research Organization (CSIRO) and Bureau of Meteorology (BOM), Australia	✓	✓	✓	1.9° × 1.2°
AWI-CM-1-1-MR	Alfred Wegener Institute, Helmholtz Centre for Polar and Marine Research, Am Handelshafen 12, 27570 Bremerhaven, Germany	✓	✓	o	1.1° × 1.1°
EC-Earth3-Veg	EC-Earth-Consortium	✓	✓	o	0.7° × 0.7°
EC-Earth3	EC-Earth-Consortium	✓	✓	o	0.7° × 0.7°
GFDL-ESM4	NOAA Geophysical Fluid Dynamics Laboratory	✓	✓	✓	1.3° × 1.0°
INM-CM4-8	Institute for Numerical Mathematics	✓	✓	✓	2.0° × 1.5°
INM-CM5-0	Institute for Numerical Mathematics	✓	✓	✓	2.0° × 1.5°
IPSL-CM6A-LR	Institut Pierre Simon Laplace, Paris 75252, France	✓	✓	o	2.5° × 1.3°
MIROC6	Japan Agency for Marine-Earth Science and Technology, Kanagawa 236-0001, Japan	✓	✓	✓	1.4° × 1.4°
MPI-ESM1-2-HR	Max Planck Institute for Meteorology, Hamburg 20146, Germany	✓	✓	✓	0.9° × 0.9°
MPI-ESM1-2-LR	Max Planck Institute for Meteorology, Hamburg 20146, Germany	✓	✓	✓	1.9° × 1.9°
MRI-ESM2-0	Meteorological Research Institute	✓	✓	✓	1.1° × 1.1°

resolution covering entire Ethiopia (i.e., 3°N - 15°N and 32°E - 48°E). To assess the skill of the GCMs in reproducing the observed climate extremes, the indices were calculated for a common 30-year period for which CHIRPS and CHIRTS data were both available. Hence, for each grid cell, the 23 climate extreme indices (Table 2) were calculated for the observed climate data (i.e., for the CHIRPS and CHIRTS data) and the historic GCMs climate outputs for the common 30-year period (i.e., 1983–2012). Similarly, the same climate extreme indices were calculated for the projected climate period (i.e., 2020–2100) for each GCM under each SSP. The indices were computed on High-Performance Cluster bwUniCluster 2.0.

2.3 Evaluation of models’ skill

The performance of the GCMs in reproducing the observed climate extremes was evaluated based on the Taylor diagram (Taylor, 2001). Taylor diagram is a widely used tool to evaluate how well a model matches observed climate states (Guo et al., 2018; Rao et al., 2019; Li et al., 2021; Yang et al., 2021; Liu et al., 2022). A Taylor diagram simultaneously visualizes three summary statistics: the *standard deviation* (σ) of simulated (Y) data normalized to that of the observed (X) data, the *correlation coefficient* (r) between simulated and observed data, and the *centered root mean squared error* ($RMSE_c$) between simulated and observed data (Table 3). For the Taylor diagrams, we computed the model skills of climate extreme indices over the area-averaged data across the entire grid cells for 30 years (i.e., 1983–2012).

2.4 Trend estimation and test

We used the Mann-Kendall (MK) method (Mann, 1945; Kendall, 1962; Pohlert, 2020) to test the trends in the respective climate extreme indices for both the baseline climate and future projections. The MK is a non-parametric test (i.e., the data does not have to meet the normality assumption) and widely used method because of its simplicity (Cattani et al., 2018; Esayas et al., 2018; Afuecheta and Omar, 2021; Li et al., 2021; Simanjuntak et al., 2022). The MK test determines the presence of monotonic (i.e., consistent) increasing or decreasing tendency of data in a given time. The magnitude of the trend is determined by using Sen’s slope estimator (Sen, 1968) which is a non-parametric approach to estimate the overall slope in a data series (Beyene et al., 2022; Malaekheh et al., 2022; Pervin and Khan, 2022). All the MK tests and slope estimates were computed using the “trend” R software package (Pohlert, 2020).

2.5 Partitioning sources of uncertainty in the projected climate extremes

Climate change projections usually involve three main sources of uncertainty, namely: uncertainty due to GCMs (M^t), SSPs (S^t), and internal climate variability (V). Using the method proposed by Hawkins and Sutton (2009); Hawkins and Sutton (2011), we evaluated the projected climate extreme indices from the GCMs (Table 1) under the three emission scenarios (SSPs) for the period from 2020 to 2100. For the temperature-related indices, this gives a total of 39 projections from the 13 GCMs ($N_m = 13$) and 3 SSPs

TABLE 2 List of ETCCDMI-defined precipitation and temperature extreme indices computed and evaluated in this study.

Label	Index name	Index definition	Units
TN10p	Cold nights	Percentage of days when TN < 10 th percentile: Let TN <i>ij</i> be the daily minimum temperature on day <i>i</i> in period <i>j</i> and let TN <i>in</i> 10 be the calendar day 10 th percentile centred on a 5-day window for the period. The percentage of time the period is determined where: TN <i>ij</i> < TN <i>in</i> 10	%
TX10p	Cold days	Percentage of days when TX < 10 th percentile: Let TX <i>ij</i> be the daily maximum temperature on day <i>i</i> in period <i>j</i> and let TX <i>in</i> 10 be the calendar day 10 th percentile centred on a 5-day window for the period. The percentage of time the period is determined where: TX <i>ij</i> < TX <i>in</i> 10	%
TN90p	Warm nights	Percentage of days when TN > 90 th percentile: Let TN <i>ij</i> be the daily minimum temperature on day <i>i</i> in period <i>j</i> and let TN <i>in</i> 90 be the calendar day 90 th percentile centred on a 5-day window for the period. The percentage of time the period is determined where: TN <i>ij</i> > TN <i>in</i> 90	%
TX90p	Warm days	Percentage of days when TX > 90 th percentile: Let TX <i>ij</i> be the daily maximum temperature on day <i>i</i> in period <i>j</i> and let TX <i>in</i> 90 be the calendar day 90 th percentile centred on a 5-day window for the period. The percentage of time the period is determined where: TX <i>ij</i> > TX <i>in</i> 90	%
WSDI	Warm spell duration	Warm spell duration index: Annual count of days with at least 6 consecutive days when TX > 90 th percentile: Let TX <i>ij</i> be the daily maximum temperature on day <i>i</i> in period <i>j</i> and let TX <i>in</i> 90 be the calendar day 90 th percentile centred on a 5-day window for the period. Then the number of days per period is summed where, in intervals of at least 6 consecutive days: TX <i>ij</i> > TX <i>in</i> 90	days
CSDI	Cold spell duration	Cold spell duration index: Annual count of days with at least 6 consecutive days when TN < 10 th percentile: Let TN <i>ij</i> be the daily maximum temperature on day <i>i</i> in period <i>j</i> and let TN <i>in</i> 10 be the calendar day 10 th percentile centred on a 5-day window for the period. Then the number of days per period is summed where, in intervals of at least 6 consecutive days: TN <i>ij</i> < TN <i>in</i> 10	days
TXx	Max TX	Monthly maximum value of daily maximum temperature: Let TXx be the daily maximum temperatures in month <i>k</i> , period <i>j</i> . The maximum daily maximum temperature each month is then: TX <i>x_{kj}</i> = max(TX <i>x_{kj}</i>)	°C
TXn	Min TX	Monthly minimum value of daily maximum temperature: Let TXn be the daily maximum temperatures in month <i>k</i> , period <i>j</i> . The minimum daily maximum temperature each month is then: TX <i>n_{kj}</i> = min(TX <i>n_{kj}</i>)	°C
TNx	Max TN	Monthly maximum value of daily minimum temperature: Let TNx be the daily minimum temperatures in month <i>k</i> , period <i>j</i> . The maximum daily minimum temperature each month is then: TN <i>x_{kj}</i> = max(TN <i>x_{kj}</i>)	°C
TNn	Min TN	Monthly minimum value of daily minimum temperature: Let TNn be the daily minimum temperatures in month <i>k</i> , period <i>j</i> . The minimum daily minimum temperature each month is then: TN <i>n_{kj}</i> = min(TN <i>n_{kj}</i>)	°C
SU	Summer days	Number of summer days: Annual count of days when TX (daily maximum temperature) > 25°C. Let TX <i>ij</i> be daily maximum temperature on day <i>i</i> in year <i>j</i> . Count the number of days where: TX <i>ij</i> > 25°C.	days
TR	Tropical nights	Number of tropical nights: Annual count of days when TN (daily minimum temperature) > 20°C. Let TN <i>ij</i> be daily minimum temperature on day <i>i</i> in year <i>j</i> . Count the number of days where: TN <i>ij</i> > 20°C.	days
Rx1day	Max 1-day precipitation	Monthly maximum 1-day precipitation: Let RR <i>ij</i> be the daily precipitation amount on day <i>i</i> in period <i>j</i> . The maximum 1-day value for period <i>j</i> are: Rx1day <i>j</i> = max (RR <i>ij</i>)	mm
Rx5day	Max 5-day precipitation	Monthly maximum consecutive 5-day precipitation: Let RR <i>kj</i> be the precipitation amount for the 5-day interval ending <i>k</i> , period <i>j</i> . Then maximum 5-day values for period <i>j</i> are: Rx5day <i>j</i> = max (RR <i>kj</i>)	mm
SDII	Simple daily intensity	Simple precipitation intensity index: Let RR <i>wj</i> be the daily precipitation amount on wet days, w (RR = 1 mm) in period <i>j</i> . If W represents number of wet days in <i>j</i> , then: SDII <i>j</i> = $\frac{\sum_{w=1}^W RR_{wj}}{W}$	mm
R1mm	Number of wet days	Annual count of days when PRCP = nn mm, nn is a user defined threshold: Let RR <i>ij</i> be the daily precipitation amount on day <i>i</i> in period <i>j</i> . Count the number of days where: RR <i>ij</i> = nnmm	days
R10 mm	Heavy precipitation days	Annual count of days when PRCP = 10 mm: Let RR <i>ij</i> be the daily precipitation amount on day <i>i</i> in period <i>j</i> . Count the number of days where: RR <i>ij</i> = 10 mm	days
R20 mm	Very heavy precipitation days	Annual count of days when PRCP = 20 mm: Let RR <i>ij</i> be the daily precipitation amount on day <i>i</i> in period <i>j</i> . Count the number of days where: RR <i>ij</i> = 20 mm	days
CDD	Consecutive dry days	Maximum length of dry spell, maximum number of consecutive days with RR < 1 mm: Let RR <i>ij</i> be the daily precipitation amount on day <i>i</i> in period <i>j</i> . Count the largest number of consecutive days where: RR <i>ij</i> < 1 mm	days
CWD	Consecutive wet days	Maximum length of wet spell, maximum number of consecutive days with RR = 1 mm: Let RR <i>ij</i> be the daily precipitation amount on day <i>i</i> in period <i>j</i> . Count the largest number of consecutive days where: RR <i>ij</i> = 1 mm	days
R95p	Very wet days total precipitation	Annual total PRCP when RR > 95p. Let RR <i>wj</i> be the daily precipitation amount on a wet day w (RR = 1.0 mm) in period <i>i</i> and let RR <i>wn</i> 95 be the 95 th percentile of precipitation on wet days in the reference period. If W represents the number of wet days in the period, then: R95p <i>j</i> = $\sum_{w=1}^W RR_{wj}$ where RR _{wj} > RR _{wn} 95	mm

(Continued on following page)

TABLE 2 (Continued) List of ETCCDMI-defined precipitation and temperature extreme indices computed and evaluated in this study.

Label	Index name	Index definition	Units
R99p	Extremely wet days total precipitation	Annual total PRCP when RR > 99p: Let RR wj be the daily precipitation amount on a wet day w (RR = 1.0 mm) in period i and let RR $w99$ be the 99 th percentile of precipitation on wet days in the reference period. If W represents the number of wet days in the period, then: R99p $j = \sum_{w=1}^W RR_{wj}$ where $RR_{wj} > RR_{w99}$	mm
PRCPTOT	Total wet-day precipitation	Annual total precipitation in wet days: Let RR ij be the daily precipitation amount on day i in period j . If I represents the number of days in j , then PRCPTOT $j = \sum_{i=1}^I RR_{ij}$	mm

TABLE 3 Performance statistics on which the Taylor diagrams are based.

Symbol	Description	Notation
X, Y	Observed and simulated climate extreme indices	
σ_x, σ_y	Standard deviations of observed and simulated climate extreme indices	$\sigma_x = \sqrt{\frac{\sum_{n=1}^N (X_n - \bar{X})^2}{N}}$, $\sigma_y = \sqrt{\frac{\sum_{n=1}^N (Y_n - \bar{Y})^2}{N}}$
r	Correlation coefficient between observed and simulated climate extreme indices	$r = \frac{1}{N} \frac{\sum_{n=1}^N (X_n - \bar{X})(Y_n - \bar{Y})}{\sigma_x \sigma_y}$
RMSE _c	Centered root mean squared error between observed and simulated climate extreme indices	$RMSE_c = \sqrt{\frac{1}{N} \sum_{n=1}^N [(X_n - \bar{X}) - (Y_n - \bar{Y})]^2}$

($N_s = 3$). For the precipitation-related indices, the total was 27 with $N_m = 9$ and $N_t = 3$, because three GCMs simulations did not include precipitation.

The decomposition of the uncertainty was computed on the changes (denoted as $Y^{s,m,t}$) of climate extreme indices between a future and a baseline climate period for each grid cell following the studies of Hawkins and Sutton. (2011); Zhang and Chen (2021). Here, the period 1983–2012 was considered as a baseline period to calculate the changes ($Y^{s,m,t}$) due to climate change. The changes in temperature derived indices are expressed in terms of absolute changes as follows:

$$Y^{s,m,t} = P^{s,m,t} - \frac{1}{30} \times \sum_{t=1983}^{2012} P^{s,m,t} \tag{1}$$

and the changes in precipitation-related extreme indices are defined as percentage ratio:

$$Y^{s,m,t} = 100 \times \left(\frac{P^{s,m,t}}{\frac{1}{30} \times \sum_{t=1983}^{2012} P^{s,m,t}} - 1 \right) \% \tag{2}$$

where $s = 1, \dots, N_s$, $m = 1, \dots, N_m$, and $t = 1, \dots, N_t$ refer to the number of SSPs, GCMs, and years, respectively, and $P^{s,m,t}$ refer to the projected extreme indices for the s^{th} SSPs, m^{th} GCM, and t^{th} year.

Subsequently, the resulting changes ($Y^{s,m,t}$) were then smoothed into rolling decadal (i.e., 10 years) means and subjected to uncertainty decomposition. The uncertainty decomposition procedures are summarized as follows. To quantify and decompose the uncertainty, the smoothed mean change ($Y^{s,m,t}$) for all GCMs and SSPs was partitioned into a climate change signal (the smooth fit, $i^{s,m,t}$) and a residual ($\epsilon^{s,m,t}$) by fitting fourth-order and second-order polynomial models to precipitation and temperature indices, respectively (Hawkins and Sutton, 2011; Zhang and Chen, 2021).

$$Y^{s,m,t} = i^{s,m,t} + \epsilon^{s,m,t} \tag{3}$$

The respective means of $i^{s,m,t}$ and $\epsilon^{s,m,t}$ were calculated as follows (Eqs. 4–6); (Eq. 7):

$$\bar{i}_{s,t}^M = \frac{1}{N_m} \sum_{m=1}^{N_m} i^{s,m,t} \tag{4}$$

$$\bar{i}_s^{m,t} = \frac{1}{N_s} \sum_{s=1}^{N_s} i^{s,m,t} \tag{5}$$

$$\bar{i}_{s,M}^t = \frac{1}{N_m \times N_s} \sum_{s=1}^{N_s} \sum_{m=1}^{N_m} i^{s,m,t} \tag{6}$$

$$\bar{\epsilon} = \frac{1}{N_m \times N_s \times N_t} \sum_{s=1}^{N_s} \sum_{m=1}^{N_m} \sum_{t=1}^{N_t} \epsilon^{s,m,t} \tag{7}$$

The component of the uncertainty due to the GCMs was then estimated as the variance of the multi-scenario averages:

$$M^t = \frac{1}{N_m} \sum_{m=1}^{N_m} (\bar{i}_s^{m,t} - \bar{i}_{s,M}^t)^2 \tag{8}$$

Likewise, the component of the uncertainty due to the SSPs was then estimated as the variance of the multi-model averages:

$$S^t = \frac{1}{N_s} \sum_{s=1}^{N_s} (\bar{i}_{s,M}^t - \bar{i}_{s,M}^t)^2 \tag{9}$$

On the other hand, the uncertainty due to the internal climate variability corresponds to the variance of the residuals from the fits over all GCMs, SSPs, and projection period (i.e., 2020–2095, $N_t = 75$).

$$V = \frac{1}{N_m \times N_s \times N_t} \sum_{s=1}^{N_s} \sum_{m=1}^{N_m} \sum_{t=1}^{N_t} (\bar{\epsilon} - \epsilon^{s,m,t})^2 \tag{10}$$

In our present study, we assumed no interaction effects between GCMs and SSPs, and equal weights were given for all GCMs despite the different performances (Zhang and Chen, 2021). The total uncertainty (T^t) is, therefore, the sum of the uncertainty due to GCMs, SSPs, and internal climate variability.

$$T^t = S^t + M^t + V \tag{11}$$

The signal-to-noise (S/N) ratio was calculated to understand the influence of uncertainties on projected climate extreme indices over time (Hawkins and Sutton, 2009).

$$(S/N)^t = \frac{\bar{i}^t}{1.65 \times \sqrt{T^t}} \quad (12)$$

A larger S/N ratio implies that the projected uncertainties are smaller relative to the average climate change signal (Hawkins and Sutton, 2011; Zhang et al., 2011). The uncertainty of projected climate extreme indices was analyzed for the nine sub-regions (denoted as R1-R9) of Ethiopia that were identified based on homogeneous rainfall zones by Rettie et al. (2023).

3 Results and discussion

3.1 Temperature indices

Measuring the performance of the climate models in capturing the observed climate extreme indices is an important part of climate studies. Figure 2 shows the Taylor diagrams comparing the performance of the GCMs and their ensemble average in reproducing the different temperature extreme indices in the observation data (i.e., CHIRPS and CHIRTS) during 1983–2012. For most of the temperature-related extreme indices, the correlation coefficients range from 0.2 to 0.60. A larger range of correlation coefficients is found for extremes such as TN10p, TX90p, TN10p, TN90p, SU, and TR (refer Table 2). For absolute temperature indices like TNn, TXn, WSDI, and CSDI, the correlation coefficients (r) are very low. However, the interannual variation expressed by the standard deviations (SD) of the observation was well reproduced by most of the GCMs. Most of the indices simulated were well below 1.5 SD relative to the SD of the observations. For TX10p, WSDI and CSDI indices, many of the GCMs produced lower variability compared to the observations. The diagrams also show that the centered RMSE is well below 1.5 units relative to the SD of observations. The smallest error was found for TX90p and TX10p. The centered RMSE quantified the differences in two fields, in our case the indices in the observation data and the indices simulated by the GCMs. The diagram further shows that the GCMs ensemble average reduced both the errors (centered RMSE) and the interannual variability (SD) while the correlation coefficients (r) were increased for majority of the temperature-related indices indicating that the GCMs ensemble average performance was better than individual GCMs. The individual model as well as their ensemble average performance also varied at the regional level (Supplementary Figures S1, S2). In their multi-model study in China, Wei et al. (2022) also reported that GCMs ensemble averages of climate extreme outperform those by individual models. The models' skill was much better for the drier and hotter sub-regions (i.e., R1, R2, and R4) compared to the cooler highland regions. More importantly, the improvement from the GCMs ensemble average was more pronounced at the regional scale (Supplementary Figure S2).

Figures 3–5 show the spatial distribution of annual trends in temperature-related extreme indices in the projected climate (2020–2100) under the three SSPs in comparison to the corresponding trends in the observed climate (1982–2012). The figures clearly show significant trends in both observations and projections for all indices except for projected cold spell duration indices (CSDI). Looking at the percentile indices, higher warm extreme indices (TX90p and TN90p) are expected in future climate ranging from 4% (SSP2-4.5) to 10% (SSP5-8.5) per decade compared to approximately 3% per decade increase in the observation period. Based on the CHIRPS data (i.e., the same observed data as in our study), Gebrechorkos et al. (2019b) reported similar patterns of extreme temperature trends for the pasty climate (1979–2010). Changes of higher magnitude of temperature extremes were reported at local level studies (Birhan et al., 2022). The increasing trend in warm extreme indices is confirmed by increasing trends in other warming indicators such as summary days (SU), tropical nights (TR), and warm spell duration (WSDI). The number of summer days (SU) and tropical nights (TR) are expected to increase by up to 35 days and 50 days, respectively, particularly in the highland regions under the SSP5-8.5 scenario. Similar increasing trends are expected for the warm spell duration index (WSDI), which could increase by up to 45 days per decade under the SSP5-8.5 scenario. The results also indicate that the magnitude the warm percentile indices expected to increase would be higher than the magnitude the cold percentile indices are expected to decrease. The relatively stronger downward trend of cold extreme indices (i.e., TX10p and TN10p) over the observation period (~4% per decade) is expected to decrease in future climate by ~1% per decade under the SSP5-8.5 scenario. On the other hand, the absolute extreme maximum and minimum temperature indices (TXx, TXn, TNn, and TNx) show spatially heterogeneous patterns, not solely, but particularly in the observations. However, largely significant increasing trends of the absolute extreme maximum and minimum temperature indices are expected in the future climate, especially under the higher emission scenarios (SSP3-7.0 and SSP5-8.5). For instance, under the SSP5-8.5 emission scenario, the predicted absolute maximum of maximum temperature (TXx) and minimum of minimum temperature (TNn) trends could reach up to 6°C (8°C) per decade in the warmest (northeastern) region of the country (see Figure 1). This is a very relevant finding since a few incidences of such magnitude of extreme temperatures have harmful effects on crop growth (He and Chen, 2022) and would have a devastating impact on crop yields (Vogel et al., 2019). As to be expected, the projected trends consistently increase from lower (SSP2-4.5) to higher (SSP5-8.5) emission scenarios.

3.2 Precipitation indices

The Taylor diagrams in Figure 6 indicate the performance of the individual GCMs with respect to the precipitation-related extreme indices in the observation data (i.e., CHIRPS) during 1983–2012. The GCMs had difficulties reproducing the observed data even at the sub-regional level (Supplementary Figures S3, S4). The correlation coefficients (r) of most precipitation-related extreme indices were below 0.4. The simulated variability in precipitation was considerably higher than the observed one

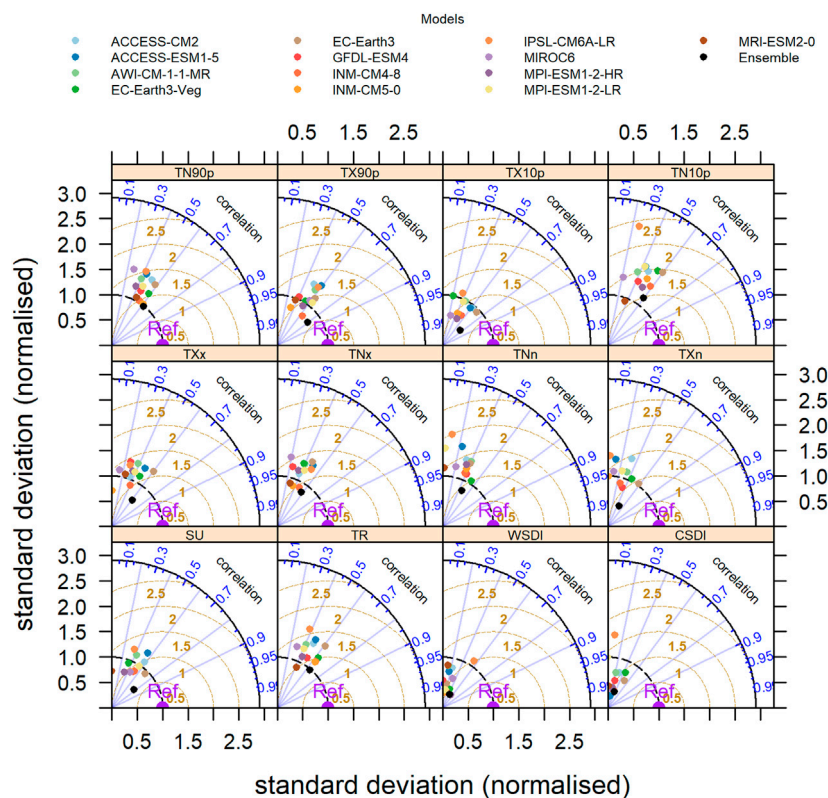


FIGURE 2

Taylor diagrams comparing the skill of the Global Climate Models (GCMs) in reproducing the observed (1983–2012) temperature related indices. The azimuthal axis shows the correlation coefficients. The radial distance from the origin represents the variability (SD), while the distance from the “Ref” point is the centered RMSE (brown dashed lines) difference between the GCMs and observed temperature related indices.

where the standard deviations normalized to the observations are mostly around 2, with R20mm, R95pTOT, and R99pTOT showing values up to 3. The errors between the GCMs and the observation (*centered RMSE*) were within 2 units. The diagrams reveal that the GCMs ensemble average reduced both the error (*centered RMSE*) and the interannual variability (SD). However, for the majority of the indices, the correlation coefficients did not improve. Overall, regarding the precipitation-related indices, the GCMs performed much less well than for the temperature-related indices. The spatial distribution of the trend in precipitation-related extreme indices in the observed climate (1982–2012) and the projected climate (2020–2100) under the three SPSs are presented in Figures 7–9. The spatial patterns show that the observed trends were largely statistically significant (i.e., shown as areas with patches) across most of the indices except for R1mm, R10mm, R20mm, and Rx5day for some pocket areas in the western and southeastern parts of the country. The southeastern part of the country which belongs to the driest regions of the country [see Figure 1A; also refer to Rettie et al. (2023)] exhibited a significant increase in maximum 5-day precipitation (Rx5day), which is equivalent to an increase of 10 days per decade. Beyene et al. (2022) also found a significantly increasing trend in Rx5day the southern region, mainly Omo-Gibe and Rift Valley lake basins. Whereas the western part

bordering Sudan showed a significantly increasing number of wet days (R1mm) by roughly 5 days per decade. The trends in number of wet days were however not significant in all scenarios. Largely increasing trends were also reported in Beyene et al. (2022) for R10 mm indices for Ethiopia of which 20% of the grids were statistically significant. Cattani et al. (2018) analyzed seasonal rainfall variability and trends over East Africa for 1983–2015. They found that R1mm and R20 mm show decreasing trend during October–December and an increasing trend during March–May seasons for the larger part of East Africa. On the other hand, as in the observed climate, significantly increasing trends are projected for maximum 5-day precipitation (Rx5day) where the trends were significant across the large parts of the country. Likewise, generally increasing trends were projected for number of days with more than 10 mm (R10 mm) and 20 mm (R20 mm) indices. They were significant across large parts of the country. Regarding the precipitation totals and wet days, exceptionally higher increases were projected under SSP3-7.0 in a small pocket region in the northwestern part of the country, which was statistically significant as well (Figure 9). The projected change for the indicated pocket region was more than 25 days per year increase both for very wet (R95pTOT) and extremely very wet (R99pTOT) days. Our results are in line with Gebrechorkos et al.

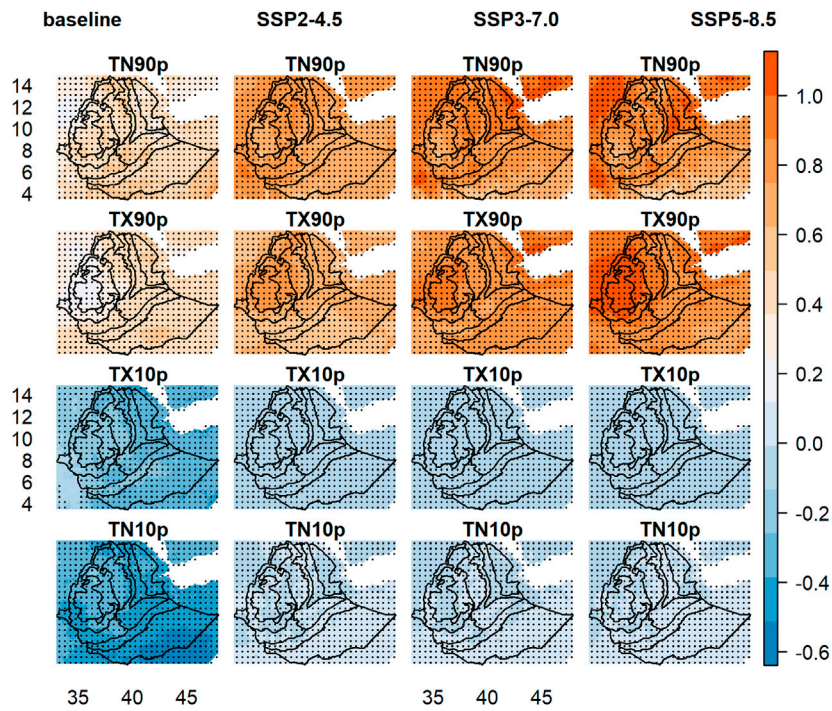


FIGURE 3
 Spatial distribution of annual historical (1983–2012) and projected (2020–2100) trends (Sen’s slope) in multi-GCMs averaged temperature indices (TN90p, TX90p, TX10p, and TN10p in % units) under the three SSPs. The areas under patches (depicted as signs) show significant ($p < 0.05$, MK test) trends.

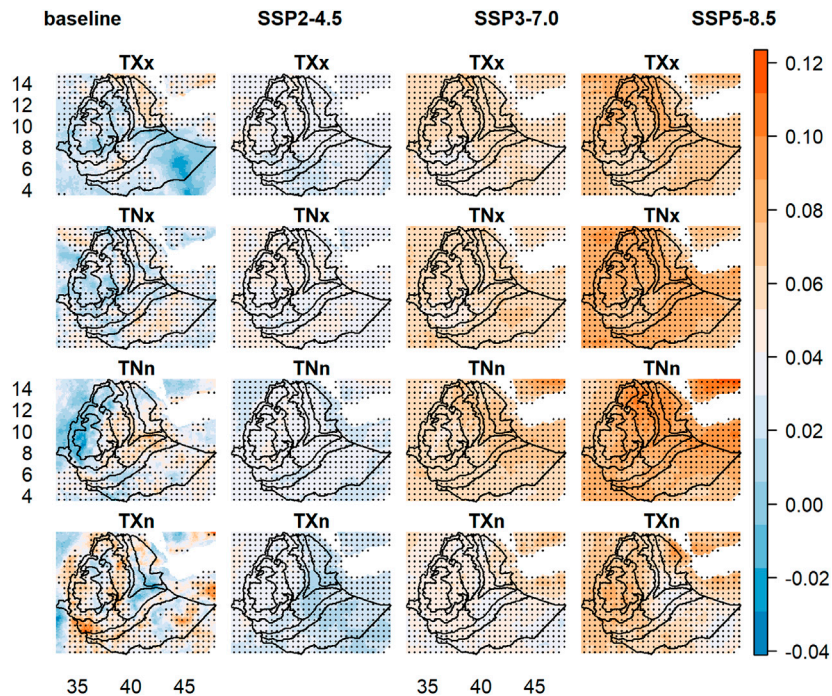


FIGURE 4
 Same as Figure 3 but for indices: TXx, TNx, TNn and TXn in °C.

(2019a), who found a significantly increased trend in R99pTOT and R99pTOT in southern Ethiopia for the period of 1981–2010. Unlike the temperature indices, the trends in precipitation are

generally heterogeneous in terms of spatial distribution, magnitude, and statistical significance as well as across the different emission scenarios (SSPs). Despite the large spatial

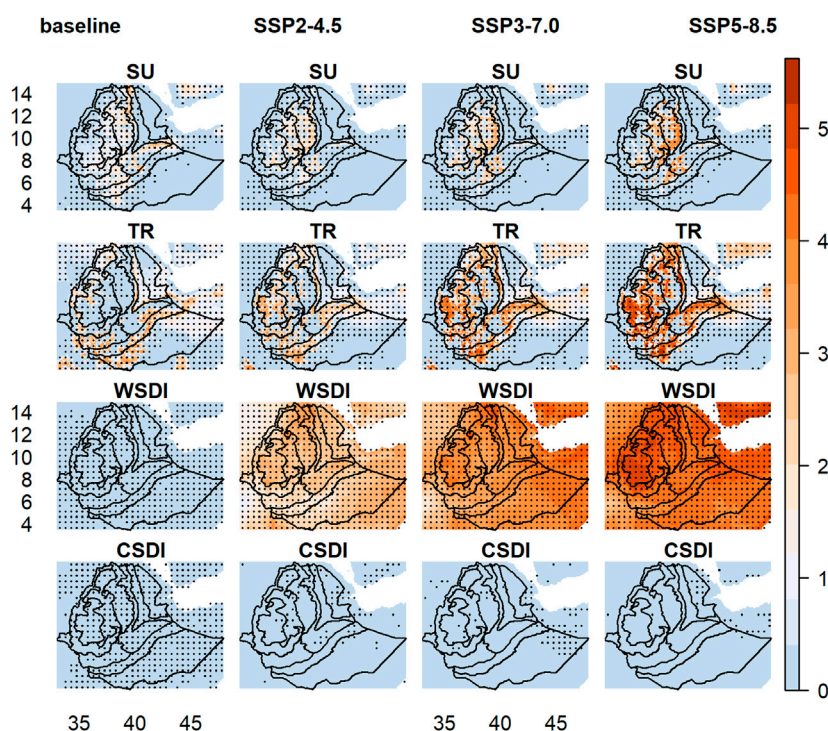


FIGURE 5
Same as Figure 3 but for indices: SU, TR, WSDI and CSDI in days.

inconsistency, the overall results suggested that there are indications for an increase in the frequency of the most intense precipitation events.

3.3 Projection uncertainty

We assessed the three components of climate change uncertainty (i.e., model (GCM), scenario (SSP), and internal climate variability) for all climate extreme indices for the 9 sub-regions defined by Rettie et al. (2023); Figures 10–13 present the evolution of the three components over time for the temperature-related indices (Figure 10; Figure 11) and precipitation-related indices (Figure 12; Figure 13). The figures show that, for temperature-related indices, a general decreasing contribution of uncertainties from the GCMs and internal variability to the total uncertainty while the reverse was true for the uncertainty from SSPs. These findings were largely consistent across the different regions of the country. Accordingly, the uncertainty from the GCMs accounts for about 64%–88% of the total uncertainty at the beginning of the projection period (i.e., 2020). This proportion decreased to about 45%–67% by the end of the projection period (i.e., 2100). Meanwhile, the contribution from the internal variability decreased from about 11%–32% at the beginning of the projected climate to less than 15% by the end of the century. Summer days (SU) are an exception here, with a slight projected increase. On the other hand, the fraction of uncertainty from the

SSPs increased from less than 1% in 2020 to 18%–54% by the end of the century. Our results are consistent with previous studies that in the beginning projections are usually dominated by uncertainties from GCMs and internal variability (Zhang and Chen, 2021). The results were consistent across the temperature indices except for the cold spell duration index (CSDI) where the SSPs’ contribution to the total uncertainty remained negligible.

In contrast to the temperature indices, the total projection uncertainty of precipitation-related indices was dominated by the contribution from the GCMs and the internal climate variability, with marginal contribution from the SSPs. However, the fractional contribution from the GCMs and internal variability varies among the different indices. For CDD, CWD, R1mm, and Rx1day, a large proportion (~57–87%) of the total uncertainty was due to the internal climate variability whereas, for the rest of the precipitation indices, the contribution from the GCMs is considerable. Mendoza Paz and Willems. (2022) also found that the larger proportions of the uncertainty in the projected precipitation extremes were related to the GCMs. In addition, the contribution of model uncertainty increases with a lead time for most of the precipitation indices except for CDD, CWD, R1mm, and Rx1day. Results were consistent across the different sub-regions. Compared to the temperature indices, internal climate variability was an important source of uncertainty for precipitation-related indices. Previous studies also showed the relative importance of the uncertainty from

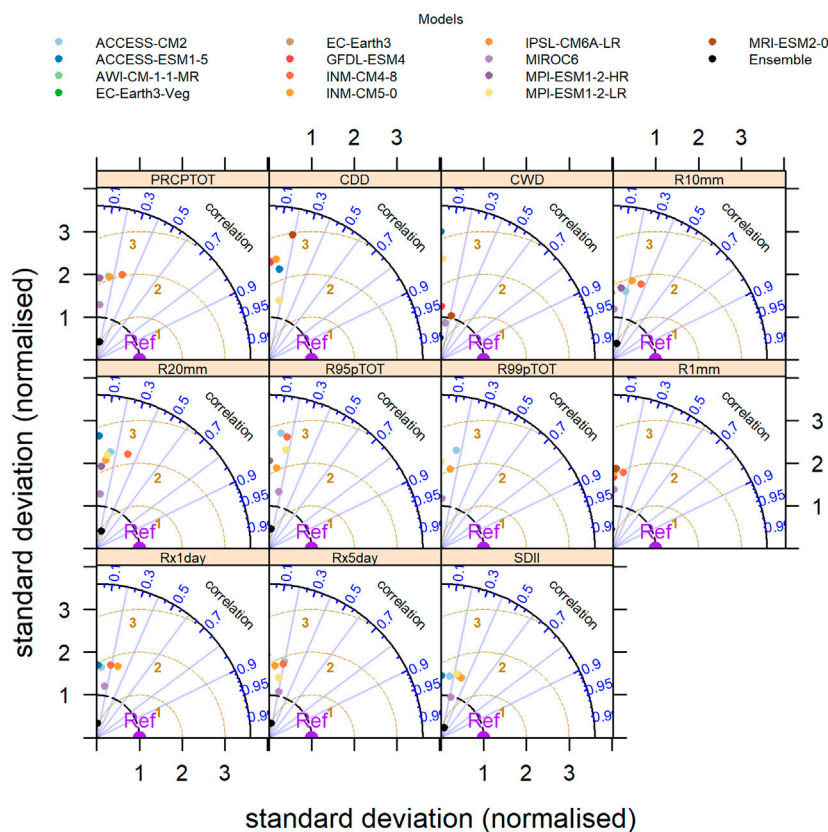


FIGURE 6
Taylor diagrams comparing the skill of the Global Climate Models (GCMs) in reproducing the observed (1983–2012) precipitation related indices. The azimuthal axis shows the correlation coefficients. The radial distance from the origin represents the variability (SD), while the distance from the “Ref” point is the centered RMSE (brown dashed lines) difference between the GCMs and observed precipitation related indices.

the internal climate variability for precipitation-related indices (e.g., Hawkins and Sutton, 2011; Fatichi et al., 2016; Gu et al., 2018).

To reduce the high uncertainty associated with the precipitation indices, we suggest further investigation based on multiple reference data sets (Grusson and Barron, 2021; Madakumbura et al., 2021) and as far as possible, station-based observation data (Cattani et al., 2018; Kim et al., 2019). Fatichi et al. (2016) claimed that the rigorous assessment of historic climate variability may give sufficient information about future changes in precipitation extremes. In addition, seasonal level analysis (Cattani et al., 2018; Ademe et al., 2020; Gemedu et al., 2021; Ali Mohammed et al., 2022; Beyene et al., 2022; Teshome et al., 2022) could also help to reduce the uncertainty compared to annual level analysis (this study) given the high spatial variability in the country.

3.4 Robustness of the projections

Finally, we quantified the signal-to-noise ratio (S/N) to demonstrate the influence of uncertainties on projected climate extreme indices over time (Hawkins and Sutton, 2009) and hence to evaluate the robustness of the projected changes in climate

extremes (Hawkins and Sutton, 2009; 2011; Zhang et al., 2011). Figure 14 and Figure 15 present the S/N ratio for the temperature and precipitation-related indices, respectively, for the different sub-regions.

Largely consistent across the temperature-related indices, the signal-to-noise values increased in general with time, but with considerable regional variation (Figure 14). This implies that the magnitude of projected changes was greater than the magnitude of the associated uncertainty and hence the projected changes are reliable. However, the S/N ratio reaches peak values by the mid of the century (i.e., between 2050–2060) for temperature intensity indices (TXx, TXn, TNx, and TNn) with slightly decreasing values with projection time. The peaks around the mid of the century could be related to the shift in the contribution of uncertainties from the different sources (i.e., GCMs, SSPs, and internal climate variability). Zhang et al. (2011) reported a similar period where the shift in the contribution of uncertainty among the various sources occur. Regional comparisons show that sub-region R8 (which is the wettest region in the country, cf. Rettie et al. (2023)) shows a higher S/N ratio for most of the temperature-related indices while sub-region R1 (which belongs to the driest regions in the country) shows relatively lower S/N, particularly for coldness indices (i.e., CSDI, and TX10p).

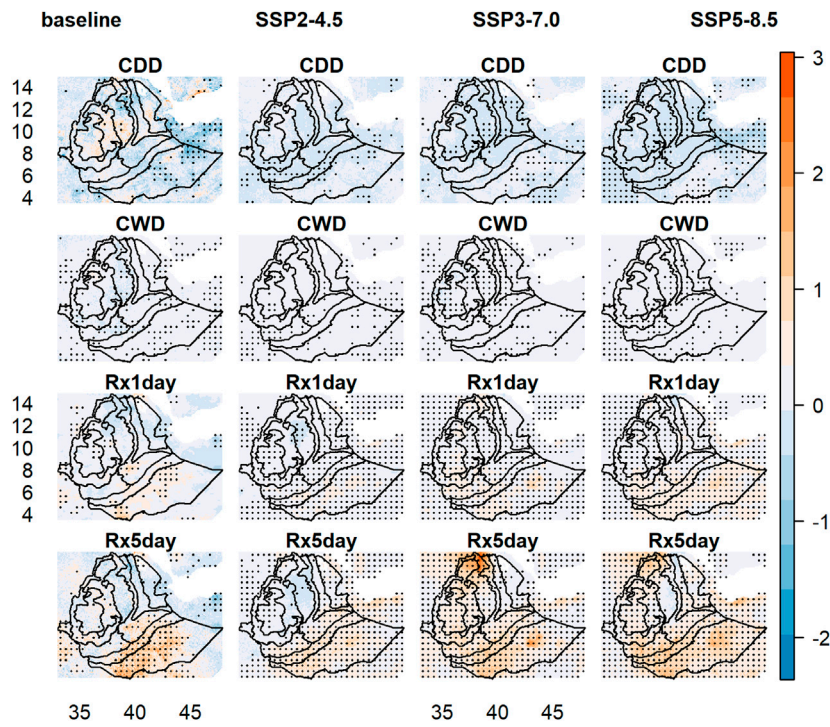


FIGURE 7 Spatial distribution of observation (1983–2012) and projected (2020–2100) trends (Sen’s slope) in multi-GCMs averaged precipitation indices (CDD and CWD in days, and Rx1day and Rx5day in mm) under the three SSPs. The patches show significant ($p < 0.05$, MK test) trends.

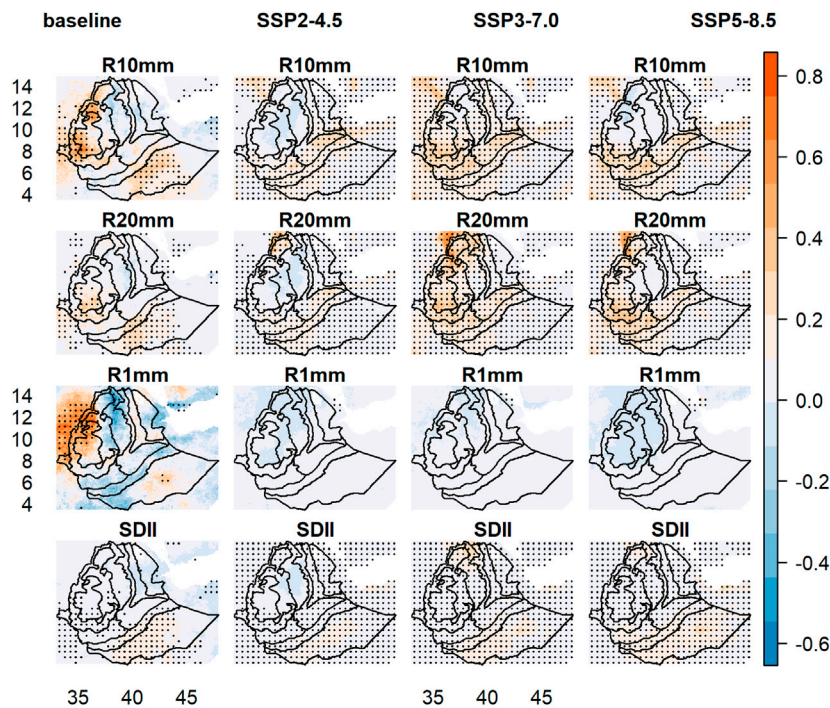


FIGURE 8 Same as Figure 7 but for indices: Number of heavy precipitation days with at least 10 mm (R10 mm) and 20 mm (R20 mm), number of wet days (R1mm), and simple daily intensity (SDII, mm).

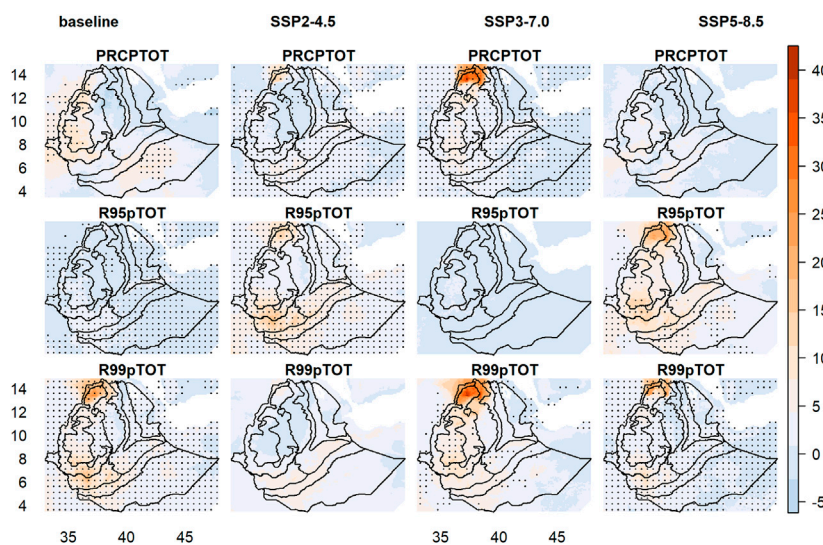


FIGURE 9 Same as Figure 7 but for indices: Total wet-day precipitation (PRCPTOT), very wet days total (R95pTOT), and extremely wet days total (R99pTOT) all in mm.

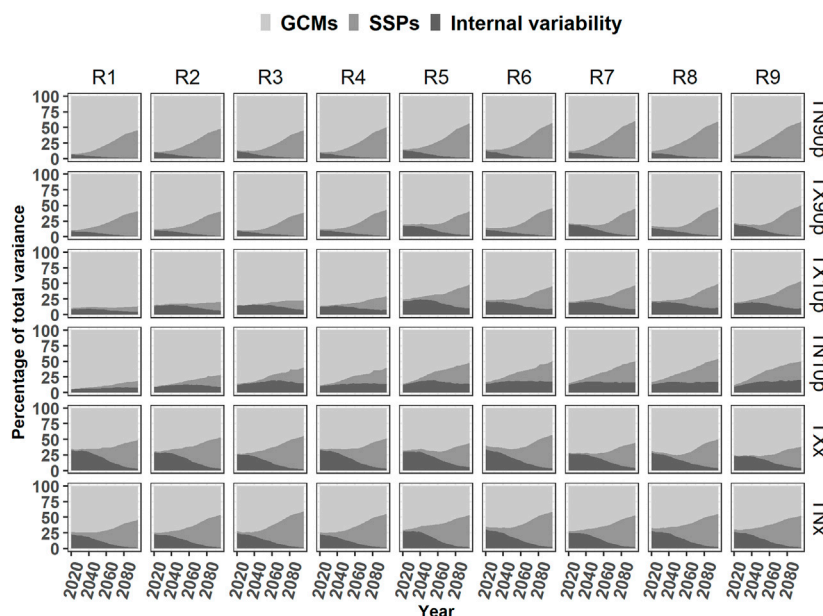


FIGURE 10 Percentage share of uncertainty for temperature indices depicted by sub-regions over 2020–2100.

Precipitation-related extremes are key for climate change adaptation as the country’s economy is heavily dependent on rainfed agriculture. The S/N ratio was below unity despite a slight increment with projection time (Figure 15) for most of the precipitation indices indicating that the magnitude of projected changes was smaller than the associated uncertainty. This implies

that the projected changes are associated with high uncertainty and make the projection less reliable and not well-suited as a basis for decision-making. Achieving reliable projections for precipitation has been a challenge due to its associated higher uncertainties compared to temperature (Madakumbura et al., 2021; Zhang and Chen, 2021; Birhan et al., 2022). On the other hand, located near the

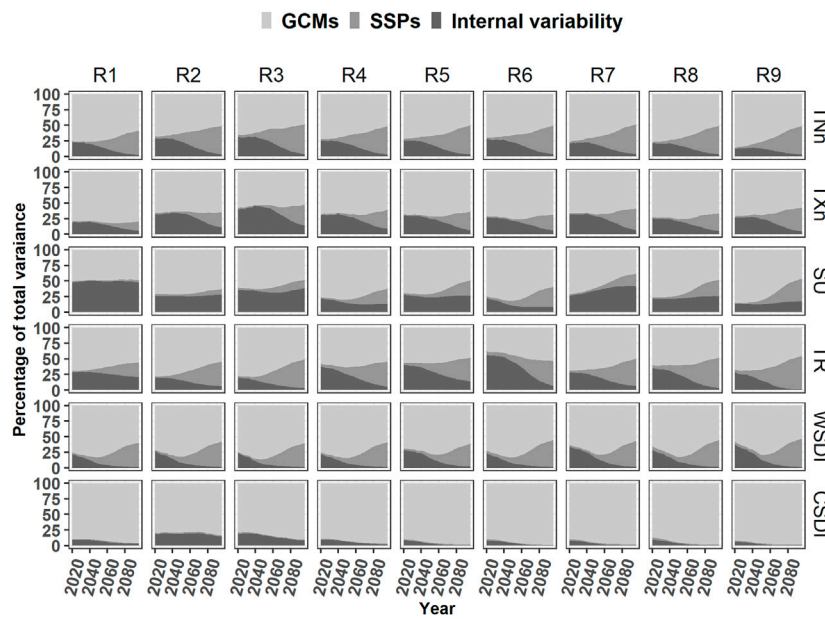


FIGURE 11
Same as Figure 10 but for indices: TNn, TXn, WSDI, CSDI, SU, and TR.

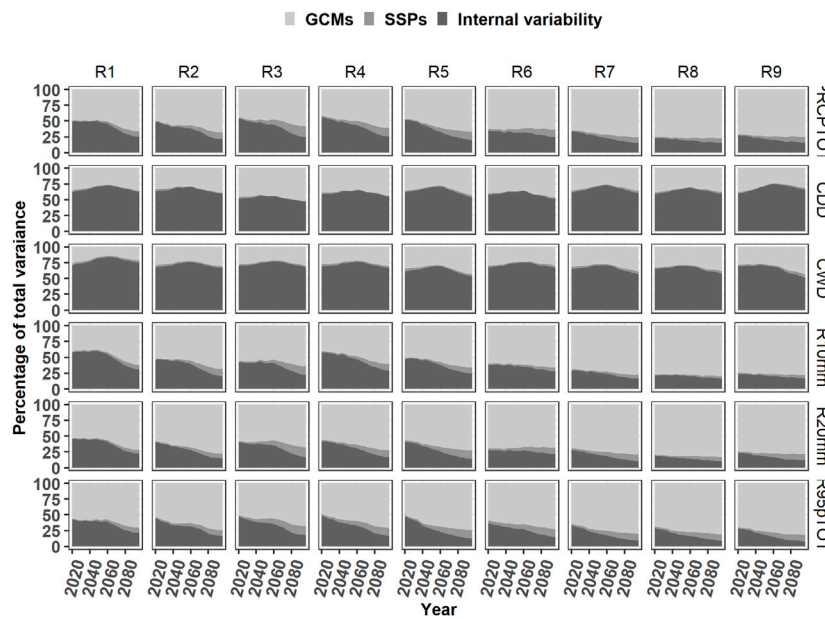


FIGURE 12
Percentage share of uncertainty for precipitation indices depicted by sub-regions over 2020–2100.

equator and the Indian Ocean, the effects of the bi-annual migration of the Inter-Tropical Convergence Zone (ITCZ) and the El Niño–Southern Oscillation (ENSO) are the most important climate systems governing precipitation across Ethiopia (Korecha and Barnston, 2007). In this regard, one of the limitations of the

current study is attributed to the structural deficiency of the climate models used in the study in reasonably simulating these major climate systems. The majority of state-of-the-art GCMs fail to simulate realistic ENSO characteristics (Beobide-Arsuaga et al., 2021) and the double- ITCZ bias remains one of the most

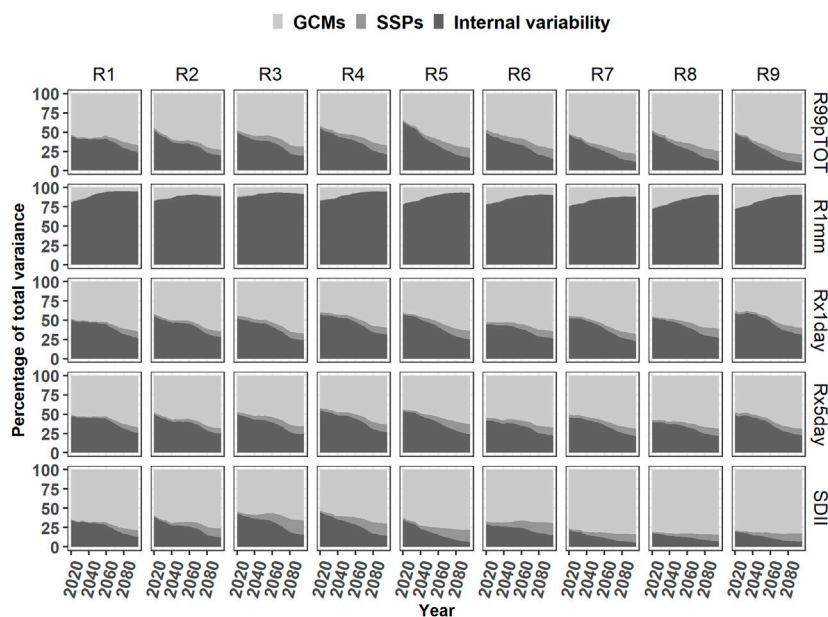


FIGURE 13
Same as Figure 12 but for indices: SDII, Rx1day, Rx5day, CDD, and CWD.

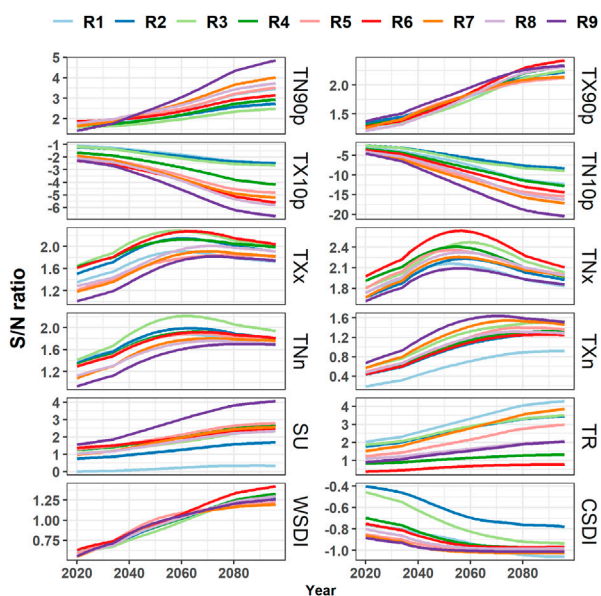


FIGURE 14
Signal-to-noise ratios for temperature indices depicted by sub-regions over 2020–2100.

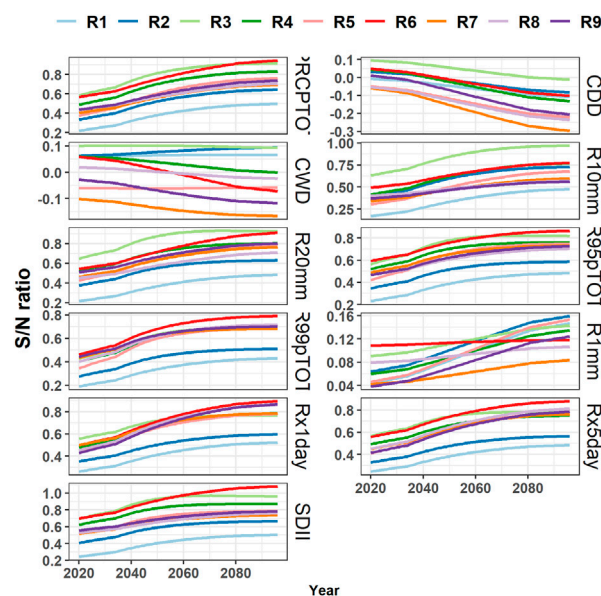


FIGURE 15
Signal-to-noise ratios for precipitation indices depicted by sub-regions over 2020–2100.

outstanding errors in the models (Tian and Dong, 2020). Given these model deficiencies, their long-term prediction of climate extremes might be affected as well. Therefore, the results of our study particularly those of precipitation-derived extreme indices should be taken with caution. Despite these limitations, the regional comparisons suggest that fewer homogeneous clusters could be sufficient for the kind of studies treated in this paper (Ware et al., 2022).

4 Conclusion

Climate extremes in Ethiopia were comprehensively assessed until the end of the 21st century by producing and evaluating a large set of extreme climate indicator indices. The study constitutes a large number of state-of-the-art CMIP6 models covering a spectrum of emission scenarios at high spatial resolution. By evaluating the

individual model performance during the base period, we estimated the possible change in the trends of projected climate extremes. The results were supplemented by a rigorous assessment of the uncertainties associated with the projected extremes. The projected trends for temperature-related indices are largely statistically significant and spatially consistent and much more reliable than the precipitation-related indices. Our study on projected changes in climate extremes at the national level was produced to serve as a baseline for future national or regional level analysis. In this context, we recommend further assessments to evaluate the effects of projected climate extremes on crop model and/or hydrological model outputs.

Data availability statement

Publicly available datasets were analyzed in this study. This data can be found here: figshare.com.

Author contributions

Conceptualization: FR, SG, and TS; methodology, formal analysis, visualization, software and validation and writing—original draft preparation: FR; supervision, investigation and resources: SG, TW, and TS; writing—review and editing: FR, SG, TW, KT, and TS; project administration and funding acquisition: SG and TS; All authors have read and agreed to the published version of the manuscript.

Funding

This publication is an output of a PhD scholarship at the University of Hohenheim in the framework of the project “German-Ethiopian SDG Graduate School: Climate Change Effects on Food Security (CLIFOOD)” between the University of Hohenheim (Germany) and the Hawassa University (Ethiopia),

References

- Ademe, D., Ziatchik, B. F., Tesfaye, K., Simane, B., Alemayehu, G., and Adgo, E. (2020). Climate trends and variability at adaptation scale: Patterns and perceptions in an agricultural region of the Ethiopian Highlands. *Weather Clim. Extrem.* 29, 100263. doi:10.1016/j.wace.2020.100263
- Afuecheta, E., and Omar, M. H. (2021). Characterization of variability and trends in daily precipitation and temperature extremes in the Horn of Africa. *Clim. Risk Manag.* 32, 100295. doi:10.1016/j.crm.2021.100295
- Alaminie, A. A., Tilahun, S. A., Legesse, S. A., Zimale, F. A., Tarkegn, G. B., and Jury, M. R. (2021). Evaluation of past and future climate trends under CMIP6 scenarios for the UBNB (Abay), Ethiopia. *WaterSwitzerl.* 13, 2110. doi:10.3390/w13152110
- Ali Mohammed, J., Gashaw, T., Worku Tefera, G., Dile, Y. T., Worqlul, A. W., and Addisu, S. (2022). Changes in observed rainfall and temperature extremes in the upper blue Nile basin of Ethiopia. *Weather Clim. Extrem.* 37, 100468. doi:10.1016/j.wace.2022.100468
- Bayable, G., Amare, G., Alemu, G., and Gashaw, T. (2021). Spatiotemporal variability and trends of rainfall and its association with Pacific Ocean sea surface temperature in west harerge zone, eastern Ethiopia. *Environ. Syst. Res.* 10, 7. doi:10.1186/s40068-020-00216-y
- Belete, M., Deng, J., Wang, K., Zhou, M., Zhu, E., Shifaw, E., et al. (2020). Evaluation of satellite rainfall products for modeling water yield over the source region of Blue Nile Basin. *Sci. Total Environ.* 708, 134834. doi:10.1016/j.scitotenv.2019.134834
- Beobide-Arsuaga, G., Bayr, T., Reintges, A., and Latif, M. (2021). Uncertainty of ENSO-amplitude projections in CMIP5 and CMIP6 models. *Clim. Dyn.* 56, 3875–3888. doi:10.1007/s00382-021-05673-4
- Berhane, G., Dereje, M., Minten, B., and Tamru, S. (2017). *The rapid—but from a low base—uptake of agricultural mechanization in Ethiopia: Patterns, implications and challenges*. Washington, D.C.; Addis Ababa, Ethiopia: International Food Policy Research Institute. Available at: <http://ebrary.ifpri.org/cdm/ref/collection/p15738coll2/id/131146>.
- Bejene, T. K., Jain, M. K., Yadav, B. K., and Agarwal, A. (2022). Multiscale investigation of precipitation extremes over Ethiopia and teleconnections to large-scale climate anomalies. *Stoch. Environ. Res. Risk Assess.* 36, 1503–1519. doi:10.1007/s00477-021-02120-y
- Birhan, D. A., Zaitchik, B. F., Fantaye, K. T., Birhanu, B. S., Damot, G. A., and Tsegaye, E. A. (2022). Observed and projected trends in climate extremes in a tropical highland region: An agroecosystem perspective. *Agroecosystem perspective* 42, 2493–2513. doi:10.1002/joc.7378
- Brown, M. E., Funk, C., Pedreros, D., Korecha, D., Lemma, M., Rowland, J., et al. (2017). A climate trend analysis of Ethiopia: Examining subseasonal climate impacts on crops and pasture conditions. *Clim. Change* 142, 169–182. doi:10.1007/s10584-017-1948-6
- Cattani, E., Merino, A., Guijarro, J. A., and Levizzani, V. (2018). East Africa Rainfall trends and variability 1983–2015 using three long-term satellite products. *Remote Sens.* 10, 931–1026. doi:10.3390/rs10060931
- IPCC (2022). “Climate change 2022: Impacts, adaptation and vulnerability,” in *Contribution of working group II to the sixth assessment report of the intergovernmental panel on climate change* Editors, D. C. Roberts, M. Tignor,

supported by the DAAD with funds from the Federal Ministry for Economic Cooperation and Development (BMZ), funding code 57316245. Additionally, this work was supported by the Collaborative Research Center 1253 CAMPOS (Project 7: Stochastic Modelling Framework), funded by the German Research Foundation (DFG, Grant Agreement SFB 1253/1 2017). The funders had no role in study design, data collection and analysis, decision to publish, or preparation of the manuscript.

Acknowledgments

The authors acknowledge the support by the state of Baden-Württemberg through bwHPC.

Conflict of interest

The authors declare that the research was conducted in the absence of any commercial or financial relationships that could be construed as a potential conflict of interest.

Publisher’s note

All claims expressed in this article are solely those of the authors and do not necessarily represent those of their affiliated organizations, or those of the publisher, the editors and the reviewers. Any product that may be evaluated in this article, or claim that may be made by its manufacturer, is not guaranteed or endorsed by the publisher.

Supplementary material

The Supplementary Material for this article can be found online at: <https://www.frontiersin.org/articles/10.3389/fenvs.2023.1127265/full#supplementary-material>

- E. S. Poloczanska, K. Mintenbeck, A. Alegría, M. Craig, et al. (Cambridge, UK; New York, NY, USA: Cambridge University Press). doi:10.1017/9781009325844
- Dendri, Z., and Birhanu, B. S. (2022). Analysis of observed trends in daily temperature and precipitation extremes in different agroecologies of gurage zone, southern Ethiopia. *Adv. Meteorology* 2022, 1–13. doi:10.1155/2022/4745123
- Dinku, T., Funk, C., Peterson, P., Maidment, R., Tadesse, T., Gadain, H., et al. (2018). Validation of the CHIRPS satellite rainfall estimates over eastern Africa. *Q. J. R. Meteorological Soc.* 144, 292–312. doi:10.1002/qj.3244
- Diro, G. T., Grimes, D. I. F., and Black, E. (2011). Large scale features affecting ethiopian rainfall. *Adv. Glob. Change Res.* 43, 1–50. doi:10.1007/978-90-481-3842-5_2
- El Kenawy, A. M., McCabe, M. F., Vicente-Serrano, S. M., López-Moreno, J. I., and Robaa, S. M. (2016). Changes in the frequency and severity of hydrological droughts over Ethiopia from 1960 to 2013. *Cuad. Investig. Geogr.* 42, 145–166. doi:10.18172/cig.2931
- Esayas, B., Simane, B., Teferi, E., Ongoma, V., and Tefera, N. (2018). Trends in extreme climate events over three agroecological zones of southern Ethiopia. *Adv. Meteorology* 2018, 1–17. doi:10.1155/2018/7354157
- Eshetu, F., and Mehare, A. (2020). Determinants of ethiopian agricultural exports: A dynamic panel data analysis. *Rev. Mark. Integration* 12, 70–94. doi:10.1177/0974929220969272
- Fatichi, S., Ivanov, V. Y., Paschalis, A., Peleg, N., Molnar, P., Rimkus, S., et al. (2016). Uncertainty partition challenges the predictability of vital details of climate change. *Earth's Future* 4, 240–251. doi:10.1002/2015EF000336
- FEWS NET (2022). Extreme food insecurity persists in the north while outcomes deteriorate in the south amid historic drought. Available at: <https://reliefweb.int/report/ethiopia/ethiopia-food-security-outlook-june-2021-january-2022>.
- Funk, C., Peterson, P., Landsfeld, M., Pedreros, D., Verdin, J., Shukla, S., et al. (2015). The climate hazards infrared precipitation with stations - a new environmental record for monitoring extremes. *Sci. Data* 2, 150066–150121. doi:10.1038/sdata.2015.66
- Gebrechorkos, S. H., Hülsmann, S., and Bernhofer, C. (2019a). Changes in temperature and precipitation extremes in Ethiopia, Kenya, and Tanzania. *Int. J. Climatol.* 39, 18–30. doi:10.1002/joc.5777
- Gebrechorkos, S. H., Hülsmann, S., and Bernhofer, C. (2019b). Long-term trends in rainfall and temperature using high-resolution climate datasets in East Africa. *Sci. Rep.* 9, 11376–11379. doi:10.1038/s41598-019-47933-8
- Gemedo, D. O., Korecha, D., and Garedew, W. (2021). Evidences of climate change presences in the wettest parts of southwest Ethiopia. *Heliyon* 7, e08009. doi:10.1016/j.heliyon.2021.e08009
- Gruson, Y., and Barron, J. (2021). Challenges in reanalysis products to assess extreme weather impacts on yield underestimate drought. *Plos Clim.* 2021, 1–11. doi:10.21203/rs.3.rs-908090/v1
- Gu, H., Yu, Z., Yang, C., Ju, Q., Yang, T., and Zhang, D. (2018). High-resolution ensemble projections and uncertainty assessment of regional climate change over China in CORDEX East Asia. *Hydrology Earth Syst. Sci.* 22, 3087–3103. doi:10.5194/hess-22-3087-2018
- Gummadi, S., Rao, K. P. C., Seid, J., Legesse, G., Kadiyala, M. D. M., Takele, R., et al. (2018). Spatio-temporal variability and trends of precipitation and extreme rainfall events in Ethiopia in 1980–2010. *Theor. Appl. Climatol.* 134, 1315–1328. doi:10.1007/s00704-017-2340-1
- Guo, L. Y., Gao, Q., Jiang, Z. H., and Li, L. (2018). Bias correction and projection of surface air temperature in LM2D multiple simulation over central and eastern China. *Adv. Clim. Change Res.* 9, 81–92. doi:10.1016/j.accre.2018.02.003
- Hamlet, A. F., Salathé, E. P., and Carrasco, P. (2010). *Statistical downscaling techniques for global climate model simulations of temperature and precipitation with application to water resources planning studies*. University of Washington, Seattle: Center for Science in the Earth System.
- Hawkins, E., and Sutton, R. (2011). The potential to narrow uncertainty in projections of regional precipitation change. *Clim. Dyn.* 37, 407–418. doi:10.1007/s00382-010-0810-6
- Hawkins, E., and Sutton, R. (2009). The potential to narrow uncertainty in regional climate predictions. *Bull. Am. Meteorological Soc.* 90, 1095–1108. doi:10.1175/2009BAMS2607.1
- He, X., and Chen, Z. (2022). Weather, cropland expansion, and deforestation in Ethiopia. *J. Environ. Econ. Manag.* 111, 102586. doi:10.1016/j.jeem.2021.102586
- Her, Y., Yoo, S. H., Cho, J., Hwang, S., Jeong, J., and Seong, C. (2019). Uncertainty in hydrological analysis of climate change: Multi-parameter vs. multi-GCM ensemble predictions. *Sci. Rep.* 9, 4974–5022. doi:10.1038/s41598-019-41334-7
- IPCC (2021). *Climate change 2021: The physical science basis. Contribution of working group I to the sixth assessment report of the intergovernmental panel on climate change*. Cambridge, UK; New York, NY, USA: Cambridge University Press. doi:10.1017/9781009157896
- Kabite Wedajo, G., Kebede Muleta, M., and Gessesse Awoke, B. (2021). Performance evaluation of multiple satellite rainfall products for Dhidhessa River Basin (DRB), Ethiopia. *Atmos. Meas. Tech.* 14, 2299–2316. doi:10.5194/amt-14-2299-2021
- Kemp, L., Xu, C., Depledge, J., Ebi, K. L., Gibbins, G., and Kohler, T. A. (2022). Climate Endgame: Exploring catastrophic climate change scenarios. *Earth, Atmos. Planet. Sci.* 119, 1–9. doi:10.1073/pnas.2108146119/-/DCSupplemental
- Kendall, M. G. (1962). *Rank correlation methods*. Oxford, England: Griffin.
- Kim, I. W., Oh, J., Woo, S., and Kripalani, R. H. (2019). Evaluation of precipitation extremes over the asian domain: Observation and modelling studies. *Clim. Dyn.* 52, 1317–1342. doi:10.1007/s00382-018-4193-4
- Kiros, F. G. (1991). Economic consequences of drought, crop failure and famine in Ethiopia, 1973–1986. *Ambio* 20, 183–185.
- Korecha, D., and Barnston, A. G. (2007). Predictability of june-september rainfall in Ethiopia. *Mon. Weather Rev.* 135, 628–650. doi:10.1175/MWR3304.1
- Lee, S., Qi, J., McCarty, G. W., Yeo, I. Y., Zhang, X., Moglen, G. E., et al. (2021). Uncertainty assessment of multi-parameter, multi-GCM, and multi-RCP simulations for streamflow and non-floodplain wetland (NFW) water storage. *J. Hydrology* 600, 126564. doi:10.1016/j.jhydrol.2021.126564
- Li, J., Miao, C., Wei, W., Zhang, G., Hua, L., Chen, Y., et al. (2021). Evaluation of CMIP6 global climate models for simulating land surface energy and water fluxes during 1979–2014. *J. Adv. Model. Earth Syst.* 13, 1–32. doi:10.1029/2021MS002515
- Liu, L. Y., Wang, X. J., Gou, X. H., Yang, M. X., and Zhang, Z. H. (2022). Projections of surface air temperature and precipitation in the 21st century in the Qilian Mountains, Northwest China, using REMO in the CORDEX. *Adv. Clim. Change Res.* 13, 344–358. doi:10.1016/j.accre.2022.03.003
- Madakumbura, G. D., Thackeray, C. W., Norris, J., Goldenson, N., and Hall, A. (2021). Anthropogenic influence on extreme precipitation over global land areas seen in multiple observational datasets. *Nat. Commun.* 12, 3944. doi:10.1038/s41467-021-24262-x
- Malakeh, S. M., Safaie, A., Shiva, L., and Tabari, H. (2022). Spatio-temporal variation of hydro-climatic variables and extreme indices over Iran based on reanalysis data. *Stoch. Environ. Res. Risk Assess.* 36, 3725–3752. doi:10.1007/s00477-022-02223-0
- Malede, D. A., Agumassie, T. A., Kosgei, J. R., Pham, Q. B., and Andualem, T. G. (2022). Evaluation of satellite rainfall estimates in a rugged topographical basin over south gojjam basin, Ethiopia. *J. Indian Soc. Remote Sens.* 50, 1333–1346. doi:10.1007/s12524-022-01530-x
- Mann, H. B. (1945). Nonparametric tests against trend. *Econ. J. Econ. Soc.* 13, 245–259. doi:10.2307/1907187
- Maurer, E. P., Hidalgo, H. G., Das, T., Dettinger, M. D., and Cayan, D. R. (2010). The utility of daily large-scale climate data in the assessment of climate change impacts on daily streamflow in California. *Hydrology Earth Syst. Sci.* 14, 1125–1138. doi:10.5194/hess-14-1125-2010
- Meinshausen, M., Nicholls, Z. R. J., Lewis, J., Gidden, M. J., Vogel, E., Freund, M., et al. (2020). The shared socio-economic pathway (SSP) greenhouse gas concentrations and their extensions to 2500. *Geosci. Model. Dev.* 13, 3571–3605. doi:10.5194/gmd-13-3571-2020
- Mendoza Paz, S., and Willems, P. (2022). Uncovering the strengths and weaknesses of an ensemble of quantile mapping methods for downscaling precipitation change in Southern Africa. *J. Hydrology Regional Stud.* 41, 101104. doi:10.1016/j.ejrh.2022.101104
- Mohammed, Y., Yimer, F., Tadesse, M., and Tesfaye, K. (2018). Meteorological drought assessment in north east highlands of Ethiopia. *Int. J. Clim. Change Strategies Manag.* 10, 142–160. doi:10.1108/IJCCSM-12-2016-0179
- Murphy, J. M., Sexton, D. M. H., Barnett, D. H., Jones, G. S., Webb, M. J., Collins, M., et al. (2004). Quantification of modelling uncertainties in a large ensemble of climate change simulations. *Nature* 430, 768–772. doi:10.1038/nature02771
- Muthoni, F. K., Odongo, V. O., Ochieng, J., Mugalavai, E. M., Mourice, S. K., Hoesche-Zeledon, I., et al. (2019). Long-term spatial-temporal trends and variability of rainfall over Eastern and Southern Africa. *Theor. Appl. Climatol.* 137, 1869–1882. doi:10.1007/s00704-018-2712-1
- Muthoni, F. (2020). Spatial-temporal trends of rainfall, maximum and minimum temperatures over West Africa. *IEEE J. Sel. Top. Appl. Earth Observations Remote Sens.* 13, 2960–2973. doi:10.1109/JSTARS.2020.2997075
- Myhre, G., Alterskjær, K., Stjern, C. W., Hodnebrog-Marelle, L., Samset, B. H., Sillmann, J., et al. (2019). Frequency of extreme precipitation increases extensively with event rareness under global warming. *Sci. Rep.* 9, 16063. doi:10.1038/s41598-019-52277-4
- O'Neill, B. C., Krieger, E., Ebi, K. L., Kemp-Benedict, E., Riahi, K., Rothman, D. S., et al. (2017). The roads ahead: Narratives for shared socioeconomic pathways describing world futures in the 21st century. *Glob. Environ. Change* 42, 169–180. doi:10.1016/j.gloenvcha.2015.01.004
- Pacific Climate Impacts Consortium (2020). *Climdex.pcic: PCIC implementation of climdex routines*. Available at: <https://CRAN.R-project.org/package=climdex.pcic>.
- Pervin, L., and Khan, M. S. M. (2022). Variability and trends of climate extremes indices from the observed and downscaled GCMs data over 1950–2020 period in Chattogram City, Bangladesh. *J. Water Clim. Change* 13, 975–998. doi:10.21666/wcc.2021.331
- Pohlert, T. (2020). Trend: Non-parametric trend tests and change-point detection. Available at: <https://CRAN.R-project.org/package=trend>.
- Rao, X., Lu, X., and Dong, W. (2019). Evaluation and projection of extreme precipitation over Northern China in CMIP5 models. *Atmosphere* 10, 691. doi:10.3390/atmos10110691

- Rettie, F. M., Gayler, S., Weber, T. K. D. D., Tesfaye, K., and Streck, T. (2023). *High-resolution CMIP6 climate projections for Ethiopia using the gridded statistical downscaling method*. Scientific Data.
- Saeidizand, R., Sabetghadam, S., Tarnavsky, E., and Pierleoni, A. (2018). Evaluation of CHIRPS rainfall estimates over Iran. *Q. J. R. Meteorological Soc.* 144, 282–291. doi:10.1002/qj.3342
- Sen, P. K. (1968). Estimates of the regression coefficient based on kendall's tau. *J. Am. Stat. Assoc.* 63, 1379–1389. doi:10.1080/01621459.1968.10480934
- Simanjuntak, C., Gaiser, T., Ahrends, H. E., and Srivastava, A. K. (2022). Spatial and temporal patterns of agrometeorological indicators in maize producing provinces of South Africa. *Sci. Rep.* 12, 12072–12118. doi:10.1038/s41598-022-15847-7
- Taye, M., Sahlu, D., Zaitchik, B. F., and Neka, M. (2020). Evaluation of satellite rainfall estimates for meteorological drought analysis over the upper blue Nile basin, Ethiopia. *Geosci. Switz.* 10, 352–422. doi:10.3390/geosciences10090352
- Taylor, K. E. (2001). Summarizing multiple aspects of model performance in a single diagram. *J. Geophys. Res. Atmos.* 106, 7183–7192. doi:10.1029/2000JD900719
- Teshome, H., Tesfaye, K., Dechassa, N., Tana, T., and Huber, M. (2022). Analysis of past and projected trends of rainfall and temperature parameters in eastern and western hararghe zones, Ethiopia. *Atmosphere* 13, 67. doi:10.3390/atmos13010067
- Tian, B., and Dong, X. (2020). The double-ITCZ bias in CMIP3, CMIP5, and CMIP6 models based on annual mean precipitation. *Geophys. Res. Lett.* 47, 1–11. doi:10.1029/2020GL087232
- Tierney, J. E., Ummenhofer, C. C., and DeMenocal, P. B. (2015). Past and future rainfall in the horn of Africa. *Sci. Adv.* 1, e1500682–e1500689. doi:10.1126/sciadv.1500682
- Van den Hende, C., Van Schaeybroeck, B., Nyssen, J., Van Vooren, S., Van Ginderachter, M., and Termonia, P. (2021). Analysis of rain-shadows in the Ethiopian Mountains using climatological model data. *Clim. Dyn.* 56, 1663–1679. doi:10.1007/s00382-020-05554-2
- Verdin, A., Funk, C., Peterson, P., Landsfeld, M., Tuholske, C., and Grace, K. (2020). Development and validation of the CHIRTS-daily quasi-global high-resolution daily temperature data set. *Sci. Data* 7, 303–314. doi:10.1038/s41597-020-00643-7
- Viste, E., Korecha, D., and Sorteberg, A. (2013). Recent drought and precipitation tendencies in Ethiopia. *Theor. Appl. Climatol.* 112, 535–551. doi:10.1007/s00704-012-0746-3
- Vogel, E., Donat, M. G., Alexander, L. V., Meinshausen, M., Ray, D. K., Karoly, D., et al. (2019). The effects of climate extremes on global agricultural yields. *Environ. Res. Lett.* 14, 054010. doi:10.1088/1748-9326/ab154b
- Ware, M. B., Mori, P., Warrach-Sagi, K., Jury, M., Schwitalla, T., Beyene, K. H., et al. (2022). Climate regionalization using objective multivariate clustering methods and characterization of climatic regions in Ethiopia. *Meteorol. Z.* 31, 431–453. doi:10.1127/metz/2022/1093
- Wei, L., Xin, X., Li, Q., Wu, Y., Tang, H., Li, Y., et al. (2022). Simulation and projection of climate extremes in China by multiple coupled model Intercomparison project Phase 6 models. *Int. J. Climatol.* 43, 219–239. doi:10.1002/joc.7751
- World Bank (2022a). Agricultural irrigated land (% of total agricultural land) - Ethiopia. Available at: <https://data.worldbank.org/indicator/AG.LND.IRIG.AG.ZS?view=chart&locations=ET>.
- World Bank (2022b). Agriculture, forestry, and fishing, value added (% of GDP) - Ethiopia. Available at: <https://data.worldbank.org/indicator/NV.AGR.TOTL.ZS?locations=ET>.
- World Bank (2022c). Employment in agriculture (% of total employment) (modeled ILO estimate) - Ethiopia. Available at: <https://data.worldbank.org/indicator/SL.AGR.EMPL.ZS?locations=ET>.
- World Bank (2022d). Health nutrition and population statistics: Population estimates and projections - Ethiopia. Available at: <https://databank.worldbank.org/source/population-estimates-and-projections>.
- Yang, X., Yong, B., Yu, Z., and Zhang, Y. (2021). An evaluation of CMIP5 precipitation simulations using ground observations over ten river basins in China. *Hydrology Res.* 52, 676–698. doi:10.2166/nh.2021.151
- Zambrano-Bigiarini, M., Nauditt, A., Birkel, C., Verbist, K., and Ribbe, L. (2017). Temporal and spatial evaluation of satellite-based rainfall estimates across the complex topographical and climatic gradients of Chile. *Hydrology Earth Syst. Sci.* 21, 1295–1320. doi:10.5194/hess-21-1295-2017
- Zhang, S., and Chen, J. (2021). Uncertainty in projection of climate extremes: A comparison of CMIP5 and CMIP6. *J. Meteorological Res.* 35, 646–662. doi:10.1007/s13351-021-1012-3
- Zhang, X., Alexander, L., Hegerl, G. C., Jones, P., Tank, A. K., Peterson, T. C., et al. (2011). Indices for monitoring changes in extremes based on daily temperature and precipitation data. *Wiley Interdiscip. Rev. Clim. Change* 2, 851–870. doi:10.1002/wcc.147